Supporting information: How important is reactor design for CO_2 conversion in warm plasmas?

Rani Vertongen[1] and Annemie Bogaerts[1]

[1] Research group PLASMANT, Department of Chemistry, University of Antwerp, Universiteitsplein 1, 2610 Antwerp, Belgium.

S1. Experimental setup: 2D scheme

We present the experimental details in section 2.1 in the main paper. Here, we provide a 2D schematic of the setup to present a clear view on the connection of all components.

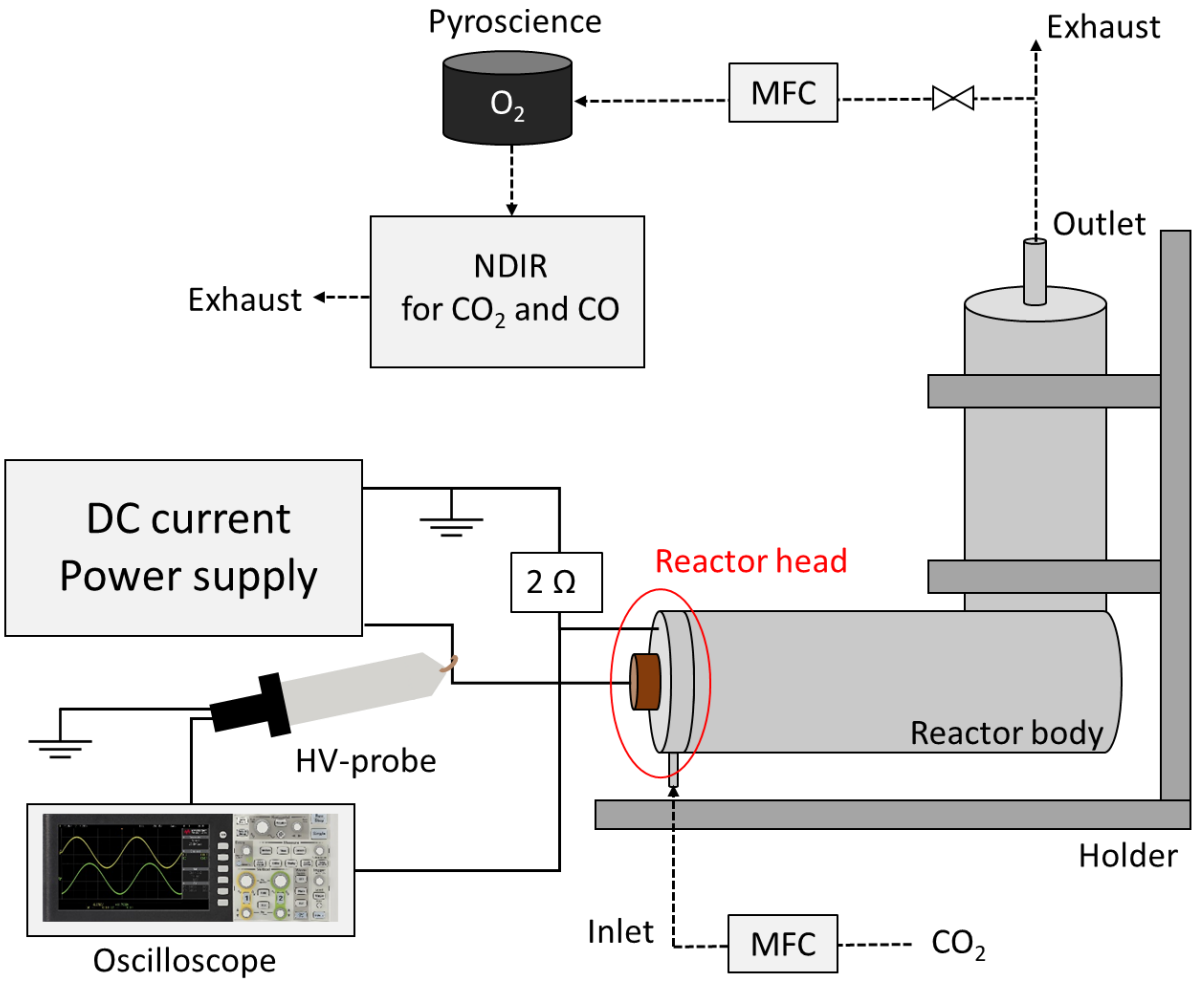

Figure SI - 1 Schematic of the experimental setup, indicating the gas circuit (dashed lines) controlled by the mass flow controller (MFC) and the electrical circuit (full lines). The reactor head is explained in more detail in Figure 2 in the main paper and previous work [1]. The reactor body has an L-shape in order to diminish the vortex flow before arriving at the diagnostics. The Faraday cage is not displayed to show each component more clearly.

S2. Overview of all electrodes and their dimensions

Table SI - 1a Overview of all GAP electrode configurations evaluated in this work. The outer shape of the electrode is displayed in dark grey, while the white space represents the gas volume. The length and diameter of the electrode are specified for each configuration, and are included in the electrode name. Unless stated otherwise, the dimensions of the electrodes are drawn to scale. The "default" reactor design that was tested by Ramakers et al. [2] is the C_{L20_d18} and A_{L16_d7} combination (indicated by the thick frame and shown in the bottom right corner).

Cathodes	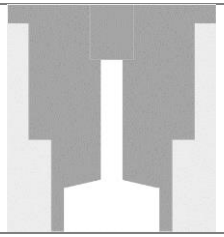	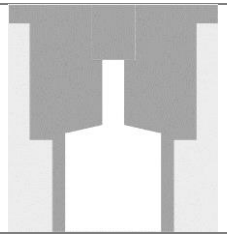	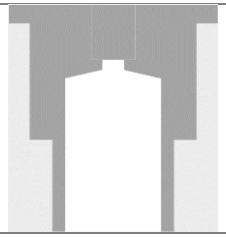	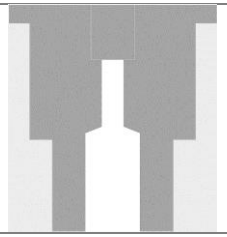	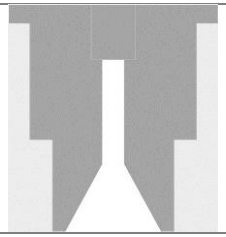
Name	C_{L10_d18}	**C_{L20_d18}**	C_{L30_d18}	C_{L20_d10}	$C_{L16\_d18\_cone}$
Length (mm)	10	20	30	20	16
Diameter (mm)	18	18	18	10	18
Anodes					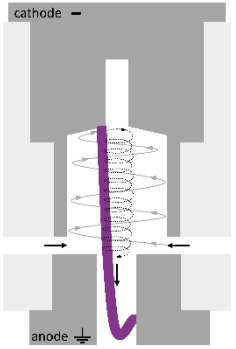
Name	$A_{L16\_d3.5}$	**A_{L16_d7}**	A_{L16_d14}	A_{L90_d7} (not on scale)	
Length (mm)	16	16	16	90	
Diameter (mm)	3.5	7	14	7	

Table SI – 1b Overview of the GAP inserted electrode configurations evaluated in this work. The picture in the right column illustrates how the inserted anodes fit into the cathode body, with schematic indication of the arc.

Inserted anodes	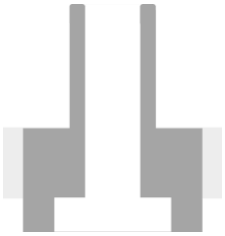	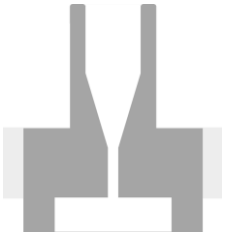		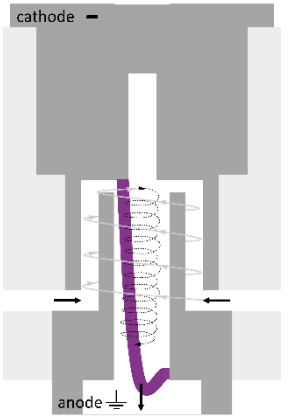
Name	$A_{insert\_L30\_d8}$	$A_{tapered\_insert\_L30\_d8}$	$A_{tapered\_insert\_L30\_d4}$	Inserted anode into cathode
Length (mm)	30	30	30	
Diameter (mm)	8	8	4	

S3. Calculation of the conversion

The conversion χ can be deduced from the stoichiometry of the reaction for pure CO_2 splitting, as indicated in Table 1.

Table 1 Reaction equation for pure CO_2 conversion, expressed in flow rates relative to the total inlet flow rate.

Reaction	**CO_2 →**	**CO**	**O_2**
in	1	0	0
out	1-χ	χ	χ/2

After the reaction, we can express the measured concentration of CO_2 as the CO_2 output fraction $y_{CO_2}^{out}$:

$$\mathrm{y}_{\mathrm{CO_2}}^{\mathrm{out}} = \frac{\dot{\mathrm{n}}_{\mathrm{CO_2}}^{\mathrm{out}}}{\dot{\mathrm{n}}_{\mathrm{tot}}^{\mathrm{out}}} = \frac{\dot{\mathrm{n}}_{\mathrm{CO_2}}^{\mathrm{out}}/\dot{\mathrm{n}}_{\mathrm{tot}}^{\mathrm{in}}}{\dot{\mathrm{n}}_{\mathrm{tot}}^{\mathrm{out}}/\dot{\mathrm{n}}_{\mathrm{tot}}^{\mathrm{in}}} = \frac{1-\chi}{(1-\chi)+\chi+\frac{\chi}{2}} = \frac{1-\chi}{1+\frac{\chi}{2}} \quad (1)$$

With $\dot{\mathrm{n}}_{\mathrm{CO_2}}^{\mathrm{out}}$ and $\dot{\mathrm{n}}_{\mathrm{tot}}^{\mathrm{out}}$ the CO_2 and total molar flow rate at the reactor outlet, respectively, and $\dot{\mathrm{n}}_{\mathrm{tot}}^{\mathrm{in}}$ the total molar flow rate at the reactor inlet (which in the case of pure CO_2 splitting is equal to the molar flow rate at the reactor inlet $\dot{\mathrm{n}}_{\mathrm{CO_2}}^{\mathrm{in}}$). For the other components, we obtain:

$$\mathrm{y}_{\mathrm{CO}}^{\mathrm{out}} = \frac{\chi}{1+\frac{\chi}{2}} \quad (2)$$

$$\mathrm{y}_{\mathrm{O_2}}^{\mathrm{out}} = \frac{\frac{\chi}{2}}{1+\frac{\chi}{2}} \quad (3)$$

The conversion is calculated from any of these measured fractions by simply rearranging the equations. When the output fraction of CO_2 is measured, we calculate the conversion as follows:

$$\chi = \frac{1-\mathrm{y}_{\mathrm{CO_2}}^{\mathrm{out}}}{1+\frac{\mathrm{y}_{\mathrm{CO_2}}^{\mathrm{out}}}{2}} \quad (4)$$

This formula inherently accounts for the gas expansion, but is only valid in pure CO_2 splitting.

S4. Effect of electrode dimensions on the measured voltage

In this section, we provide more insight in the discharge characteristics, to better understand the performance results of the various electrode designs, by studying the voltage as a function of the various design parameters. The voltage can provide insights in the length of the plasma arc, but also on the temperature of the plasma. The electrode designs change the flow pattern, which might enable better cooling of the plasma, and then the resistance of the plasma increases. At the same current, the voltage will increase according to Ohm's law. However, these trends are difficult to validate without detailed in-situ optical diagnostics, which was out of scope for this work. Therefore, the explanations in this section are meant to be indicative rather than absolute.

S4.1 Oscillographs

At a constant input current in the power supply, the voltage oscillates as a function of time, as displayed in Figure SI - 2 for three different electrode designs (i.e., the three different anode diameters). The large peaks, followed by a smaller oscillating zone, demonstrate that the arc is continuously attaching and detaching. This is in line with the properties of a gliding arc plasma and observations in previous work by our group with fast camera imaging [1].

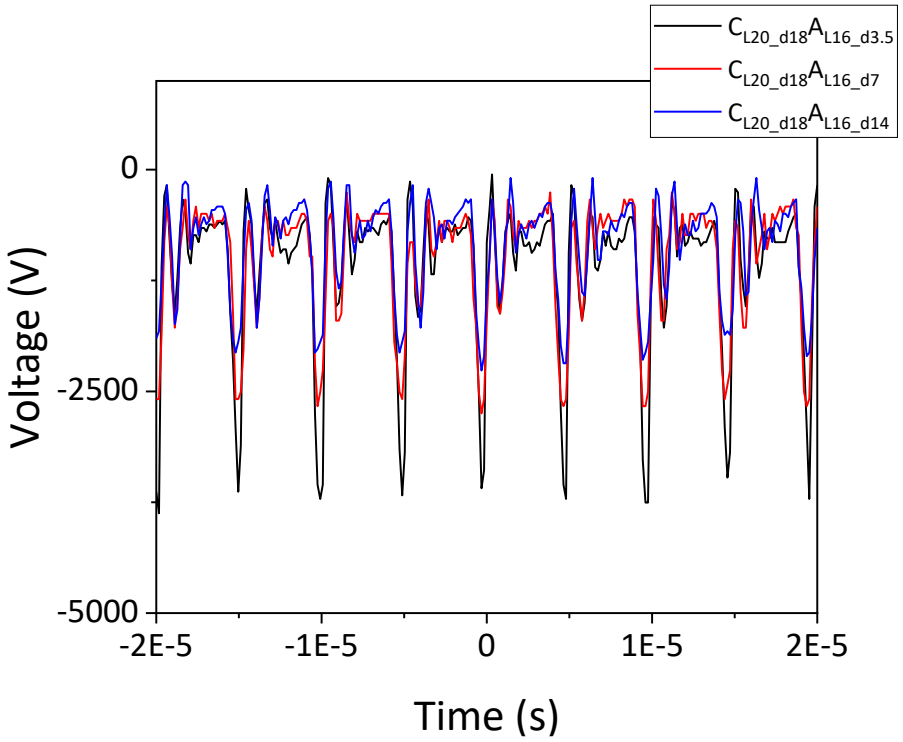

Figure SI - 2 Oscillograph, displaying the voltage as a function of time for the default cathode C_{L20_d18} and three different anodes (legend).

The smallest anode has the largest voltage peaks and seems therefore more unstable. For larger anodes, the peaks become smaller. In the next section, we will discuss this in more detail by studying the time-averaged voltage for each electrode combination.

S4.2 Effect of cathode length and anode diameter

The time-averaged voltage is plotted in Figure SI - 3 as a function of the anode diameter, for three different cathode lengths.

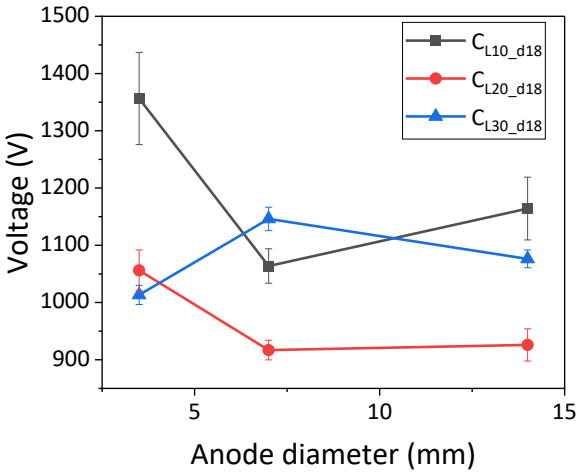

Figure SI - 3 Time-averaged voltage as a function of the anode diameter (x-axis) for three different cathode lengths (legend).

It is clear that the trend of the two shorter cathodes (C_{L10_d18} and C_{L20_d18}) are in line. The voltage remains roughly the same when decreasing the anode diameter from 14 to 7 mm, but then suddenly increases when the anode diameter drops to 3.5 mm. Probably, the arc extends more out of the reactor for a smaller anode diameter, as indeed also observed in previous work by our group for the same reactor [1]. This could explain the higher voltage, because a longer arc should correspond to a higher voltage. For the longest cathode C_{L30_d18} the trend is different: the voltage drops slightly when the anode diameter is decreased to 3.5 mm. This indicates that the plasma is contained more inside the larger cathode and thus extends less outside of the outlet when further decreasing the anode diameter.

Despite these differences in the voltage, the resulting conversion is very similar for all three cathodes, as displayed in Figure SI - 4, and the smallest outlet has the highest conversion. Indeed, independent of the cathode length, a smaller anode diameter has the most pronounced reverse vortex flow (RVF) effect, as demonstrated in previous work from our group [2, 3], which helps to improve the conversion. In addition, a smaller anode diameter also translates to a higher gas velocity at the outlet, which increases the convective cooling. This can enhance quenching once the gas leaves the reactor, similar to the effect of a nozzle after a thermal plasma, as observed by Li et al. [4]. These results indicate that for the total conversion, the anode outlet diameter, and thus the RVF effect and possible quenching effects, are more important than the time-averaged voltage.

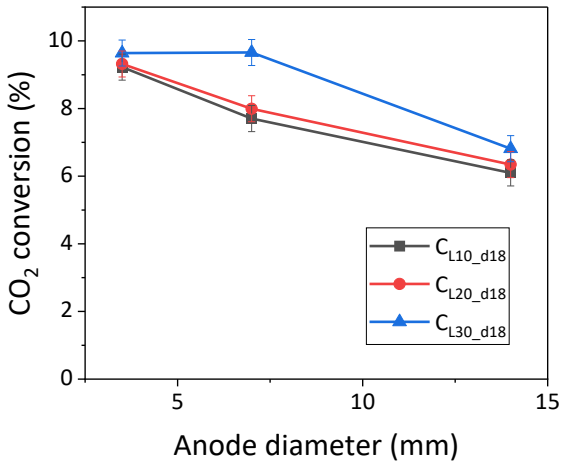

Figure SI - 4 CO_2 conversion as a function of the anode diameter (x-axis) for three different cathode lengths (legend).

S4.3 Effect of cathode and anode length

In Figure SI - 5, the time-averaged voltage is displayed as a function of the cathode length, for both the short (A_{L16_d7}) and long (A_{L90_d7}) anode.

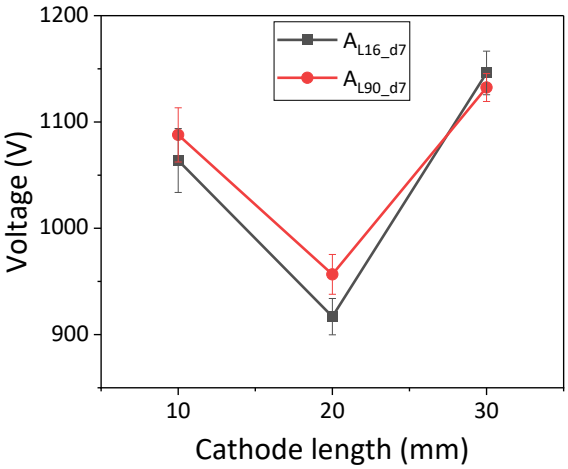

Figure SI - 5 Time-averaged voltage as a function of the cathode length (x-axis) for two different anode lengths (legend).

For both anodes, the voltage drops when decreasing the cathode length from 30 to 20 mm. Probably, the shorter cathode leads to a shorter plasma, which can explain the lower voltage. When further decreasing the cathode length to 10 mm however, the voltage increases again. Possibly, the arc extends more outside of the reactor because the smaller cathode volume cannot contain the plasma and lead to a longer afterglow.

The voltage of the longest anode is not significantly higher than for the shorter anode. There are two possible explanations for this. First, it might indicate that the plasma is not elongated significantly within the longer anode. Secondly, it is possible that the plasma is elongated in the outlet, which would increase the voltage, but that there is less cooling, which decreases the voltage again. Indeed, we observed that the configurations with the longer anode need more time to heat up before they reach a stable conversion (e.g. 7 min instead of 2 min for the shorter anodes), as discussed in the main paper. We cannot verify this just from the time-averaged voltage, but we can observe the damage from the

arc attachment on the anode: the shorter anodes show clear damage on the outlet, but this is not the case for the elongated anode. This supports our first explanation: probably, the arc is not elongated significantly in the longer anode.

Similar effects are observed for the conversion in Figure SI - 6. It is not significantly higher for the extended anode; hence, there is no improvement in the performance compared to the default design. Based on the time-averaged voltage, we thus hypothesize that the extended anode does not yield a longer arc, which is in line with our observation of no clear damage for this extended anode.

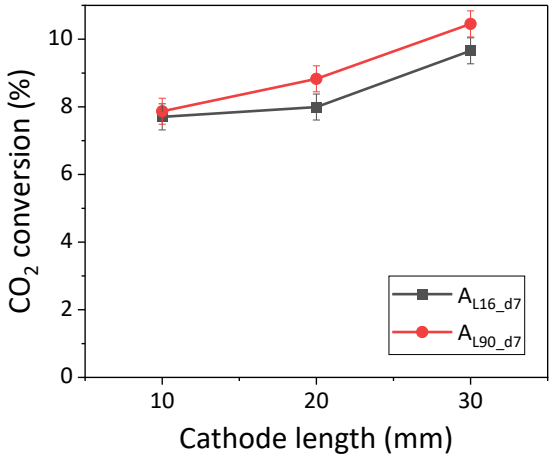

Figure SI - 6 CO_2 conversion as a function of the cathode length (x-axis) for two different anode lengths (legend).

S4.4 Effect of cathode and anode diameter

Figure SI - 7 displays the time-averaged voltage as a function of anode diameter for both the default cathode (C_{L20_d18}) and the smaller cathode diameter (A_{L20_d10}).

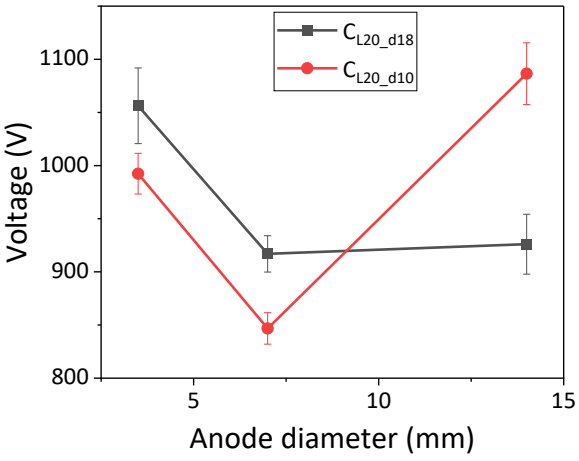

Figure SI - 7 Time-averaged voltage as a function of the anode diameter (x-axis) for two different cathode diameters (legend).

For the smaller anodes (diameter of 3.5 and 7 mm), the voltage is lower for the smaller cathode diameter. This might indicate that there is less cooling, which can indeed be expected if the distance between the hot plasma core and the walls is smaller. Then suddenly, the voltage increases for the largest anode, which might indicate that a larger anode improves the cooling. This is not the case for

the wider cathode diameter, suggesting that the properties of the discharge are indeed different depending on the cathode diameter.

If we assume that both configurations have a similar plasma length, because the cathode lengths are the same and they are combined with the same anodes, then the different voltages are a consequence only of the different cooling rates inside the cathode. Yet, the conversion is very similar for both cathodes in Figure SI - 8. This may indicate that the effects inside the cathode volume are less important than the effects at the outlet. Possibly, the conversion is largely determined by the amount of quenching at the outlet, as described in S4.2. Indeed, it has been demonstrated both experimentally [5] and my modelling [6, 7], that post-plasma quenching largely affects the overall conversion.

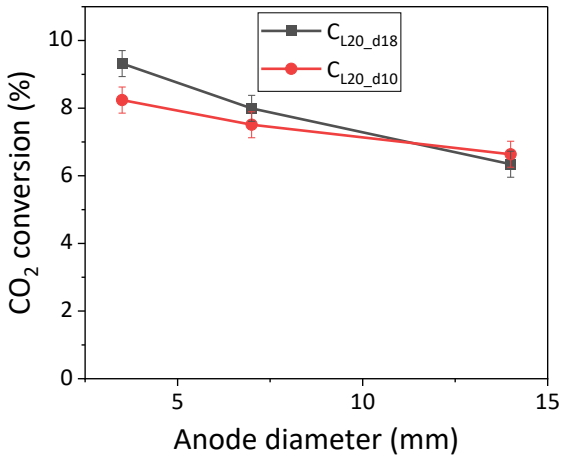

Figure SI - 8 CO_2 conversion as a function of the anode diameter (x-axis) for two different cathode diameters (legend).

S4.5 Effect of cathode shape

The time-averaged voltage is displayed in Figure SI - 9 as a function of the anode diameter for both the default cylindrical cathode (C_{L20_d18}) and for the cone-shaped cathode ($C_{L16\_d18\_cone}$).

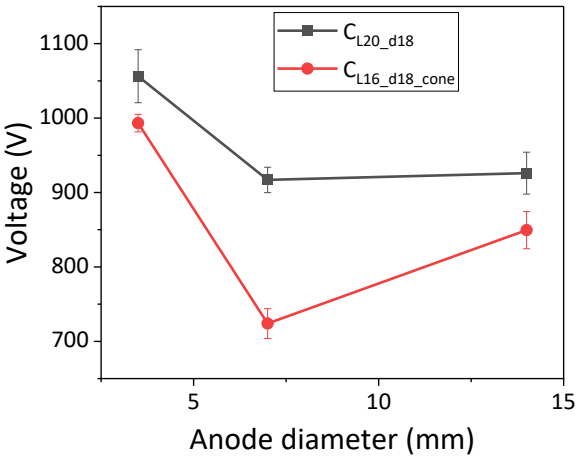

Figure SI - 9 Time-averaged voltage as a function of the anode diameter (x-axis) for two different cathode shapes (legend).

The voltage of the cone-shaped cathode is lower than that of the cylindrical cathode. Since the cone-shaped cathode is slightly shorter too, this might simply be explained by the difference in cathode length. However, the trend is very similar as for cathode with a smaller diameter (C_{L20_d10}): there is a sudden increase for the largest anode diameter, while the voltage of the cylindrical cathode remains constant. This might indicate that the cooling effects play a role again, i.e. that the cone-shaped cathode has less cooling than the cylindrical cathode.

The conversion of the cone-shaped cathode is slightly lower than that of the cylindrical cathode, as shown in Figure SI - 10. Possibly, the combined effect of the shorter cathode length and reduced cooling plays a role, explaining why the conversion is even lower than of the cathode with the smaller diameter (C_{L20_d10}) where only the cooling effects might play a role.

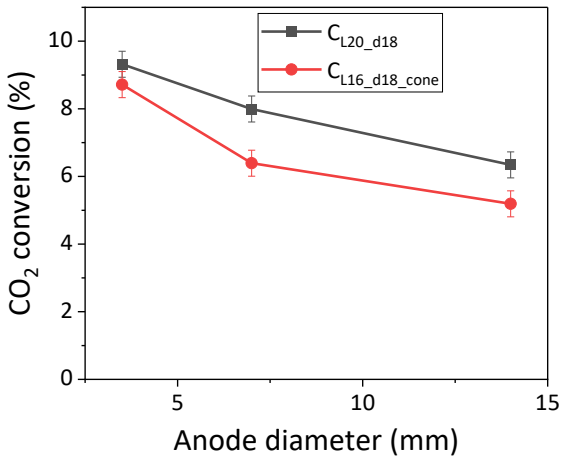

Figure SI - 10 CO_2 conversion as a function of the anode diameter (x-axis) for two different cathode shapes (legend).

S4.6 Inserted anodes

Since there is no common design parameter for the inserted anodes, we plot the time-averaged voltage as a function of the reactor volume in Figure SI - 11 for the default electrodes (C_{L20_d18}) and inserted electrodes ($C_{L16\_d18\_flat}$).

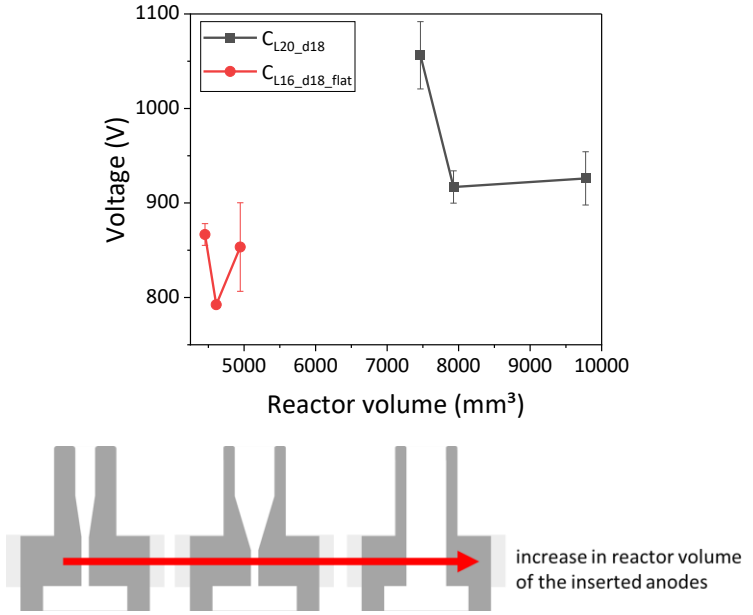

Figure SI - 11 Time-averaged voltage as a function of the reactor volume (x-axis) for the default electrode designs ($C_{L20\_d18}A_{L16\_d3.5}$, $C_{L20\_d18}A_{L16\_d7}$, $C_{L20\_d18}A_{L16\_d14}$) and the inserted electrode designs ($C_{L16\_d18\_flat}$). The increase in reactor volume for the different inserted anodes is displayed under the graph.

The voltage of the inserted anodes is lower than that of the default electrodes, which indicates that the plasma is shorter, there is less cooling or a combination of both. If the plasma does not fill the entire outlet channel, as explained in the main paper, it could form instead on the shortest distance between the cathode and the anode, as drawn in the main paper in Figure 7. In addition, the metal wall of the inserted anode inside the cathode inhibits mixing of the cold outer vortex with the warmer core, which creates a warmer plasma.

In any case, the overall stability of these electrode designs was very poor, which probably explains their low conversion, as shown in Figure SI - 12. This indicates that plasma stability is more important than plasma-gas interaction.

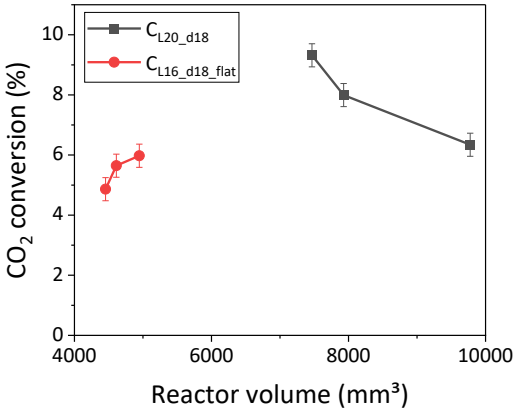

Figure SI - 12 CO_2 conversion as a function of the reactor volume (x-axis) for the default electrode designs ($C_{L20\_d18}A_{L16\_d3.5}$, $C_{L20\_d18}A_{L16\_d7}$, $C_{L20\_d18}A_{L16\_d14}$) and the inserted electrode designs ($C_{L16\_d18\_flat}$)."

S5. Effect of electrode shape on CO_2 conversion: higher flow rate

Figure SI - 13 summarises the performance, in terms of CO_2 conversion (a) and energy efficiency (b), at two different flow rates, i.e., 10 and 20 L_s/min, and for different cathode designs (i.e., different length, diameter or cone-shape), and the basic anode design. The power and specific energy input (SEI) are also plotted (see right y-axes). As expected, a higher flow rate of 20 L_s/min results in a lower conversion than at 10 L_s/min, for all cathode designs. In addition, the high flow rate yielded an unstable plasma for the smallest anode diameter ($A_{L16\_d3.5}$, not included here) and two of the cathodes (C_{L10_d18} and C_{L30_d18}). The inserted anodes were not included since higher flow rates led to a pressure build-up in the reactor.

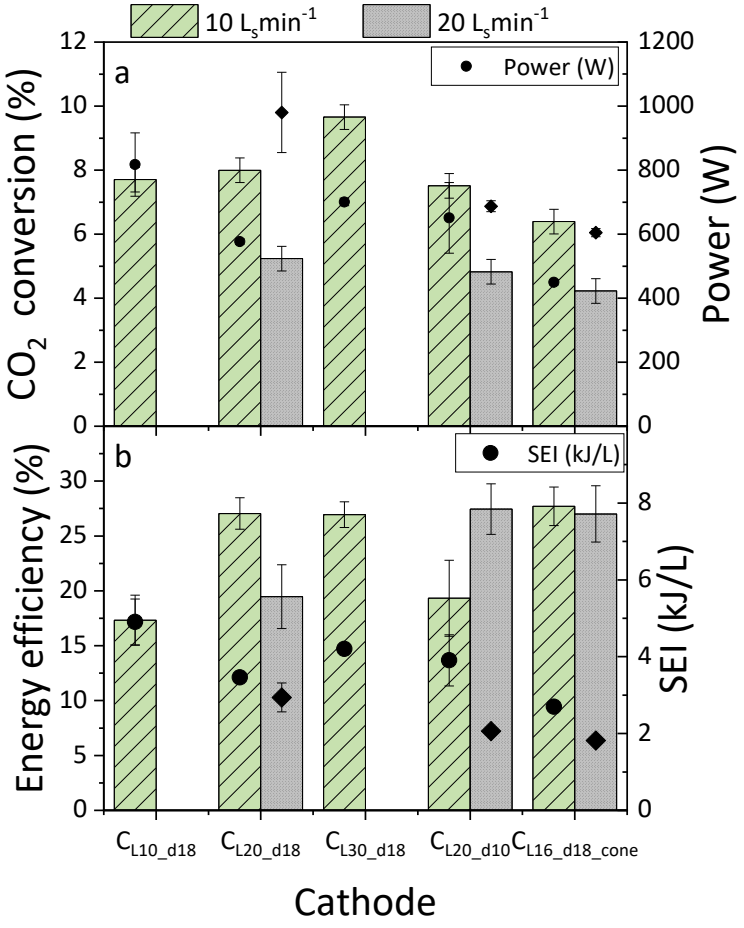

Figure SI - 13 (a) CO_2 conversion and (b) energy efficiency, presented as bars (left axis). The scatter plot represents the (a) plasma power and (b) SEI (right axis). The grouped bars represent the different cathode shapes (see x-axis), while the bar colors represent the different flow rates (see legend), all for a fixed anode A_{L16_d7} .

The higher flow rate is no guarantee for a higher energy efficiency either. For the basic cathode (C_{L20_d18}), the higher flow rate leads to a lower efficiency: the SEI is not low enough to compensate for the lower conversion. For the smaller cathode diameter (C_{L20_d10}), the higher flow rate leads to a higher energy efficiency, due to the lower SEI (indeed, similar power input but flow rate twice as high). For the cone cathode ($C_{L16\_d18\_cone}$), there is no significant difference in energy efficiency between the two flow rates. These results for the higher flow rate are included in the summarizing overview of section 4 (figure 9) in the main paper.

S6. Electrodes leading to unstable plasma and/or electromagnetic interference (EMI) issues

It is important to mention that we evaluated many more electrode shapes that were made to fit inside the same GAP reactor, with a wide range of variations in length and diameter. For a clear message in the main paper, we tried to probe the more extreme variations (e.g. the longest anode, or the cathode with the smallest possible diameter). Some electrodes were ruled out due to insights from previous work (e.g. anodes with wider diameters) [2]. In addition, some electrodes were excluded after preliminary tests that revealed unstable plasma or severe electrode damage. For the sake of transparency, and because it is useful for the reader to also learn about our "negative results", we give two examples in this section, and we explain how we dealt with the resulting electromagnetic interference (EMI) in these cases of unstable plasma.

Figure SI - 14 gives an example of two cathode configurations that gave rise to unstable plasma, i.e. the "donut" cathode and the "pin" cathode. Keep in mind that these are 2D presentations of a 3D cathode, as demonstrated on the right.

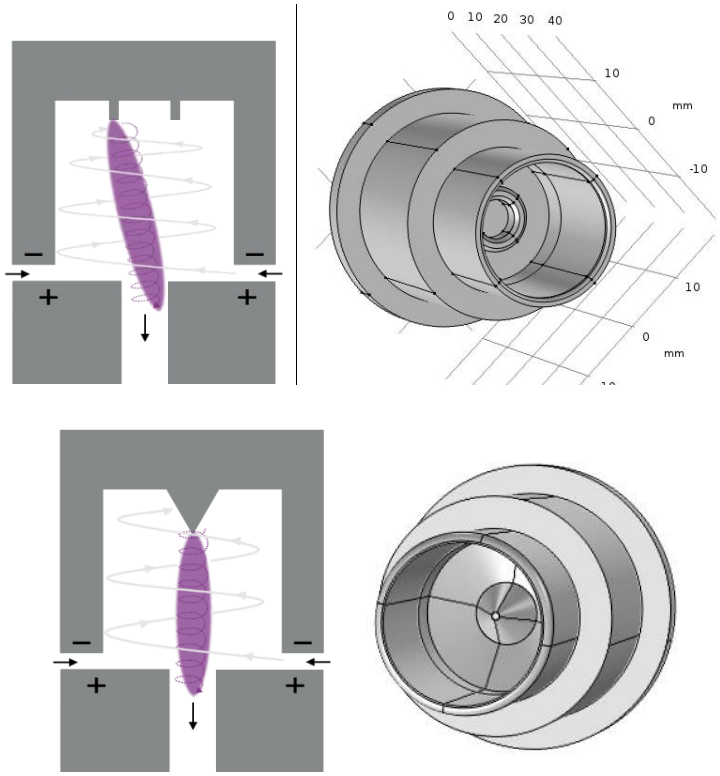

Figure SI - 14 Schematic representation in 2D (left) and 3D (right) of the donut (top) and pin (bottom) cathodes.

In both cathodes, the design idea was to play around with the location of the arc attachment. In the donut cathode, the goal was to let it rotate more in a wider volume of the cathode and thus increase the fraction of gas that is treated by the plasma. However, there was no significant difference between this cathode and the basic design. In addition, we observed significant damage in the centre of the "donut", indicating that the arc does not attach on the donut itself. Such electrode damage was even worse in the pin design. The idea here was to force an arc attachment into one point. This goal was certainly obtained, since we observed severe damage to the point. When we ran a test in the open mode (i.e. not attached to the reactor body to measure the exhaust, but open to the air to observe the plasma), the plasma was much brighter compared to the basic design, indicating that the cathode spot

is indeed much more intense. In both designs, the damage was too severe to continue the experiments, since we could not guarantee reproducibility.

These two examples, but also the inserted anodes and some operating conditions (e.g. too low power) in the other electrodes also yielded an unstable plasma. As a consequence, a lot of electromagnetic interference (EMI) was observed, with issues in nearby communication cables (e.g. USB connectors to the PC or cables from the mass flow controllers) and even an occasional shutdown of the computers in the lab. This was not an issue in the basic electrode designs, since the power supply was tailored to this type of plasma. In order to find good parameters for the flow rate and power in different electrode designs, we had to adapt the lab to account for possible EMI. Specifically, we applied the following practices for limiting EMI:

- Larger distance between the setup (power supply and reactor) and the sensitive equipment or cable.
- Routing the cables away from each other.
- Shielding the emitting device in a metal box or a Faraday cage.
- Ensuring a separate earth-ground to dissipate the EMI.
- Installing ferrite chokes as passive filters to reduce the EMI from signal or power cables.
- Reducing operating frequencies (if possible).
- Installing optocouplers in between the sensitive connections.

All of these measures are general good practices to limit the effects of interference in e.g. welding workshops, but they are also valid for plasma reactors. However, this information is usually not included in scientific literature, which makes it sometimes difficult to set up experiments for researchers who are new in the field. We hope that this short list can help plasma researchers to try and understand these issues and implement these good practices. For more information, we recommend sources on welding equipment [8] or specific literature [9].

S7. References

[1] M. Ramakers, J.A. Medrano, G. Trenchev, F. Gallucci, A. Bogaerts, Revealing the arc dynamics in a gliding arc plasmatron: a better insight to improve CO2conversion, Plasma Sources Science and Technology 26(12) (2017). https://doi.org/10.1088/1361-6595/aa9531.
[2] M. Ramakers, G. Trenchev, S. Heijkers, W. Wang, A. Bogaerts, Gliding Arc Plasmatron: Providing an Alternative Method for Carbon Dioxide Conversion, ChemSusChem 10(12) (2017) 2642-2652. https://doi.org/10.1002/cssc.201700589.
[3] G. Trenchev, S. Kolev, W. Wang, M. Ramakers, A. Bogaerts, CO2 Conversion in a Gliding Arc Plasmatron: Multidimensional Modeling for Improved Efficiency, The Journal of Physical Chemistry C 121(44) (2017) 24470-24479. https://doi.org/10.1021/acs.jpcc.7b08511.
[4] J. Li, X. Zhang, J. Shen, T. Ran, P. Chen, Y. Yin, Dissociation of CO2 by thermal plasma with contracting nozzle quenching, Journal of CO2 Utilization 21 (2017) 72-76. https://doi.org/10.1016/j.jcou.2017.04.003.
[5] A. Hecimovic, F.A. D'Isa, E. Carbone, U. Fantz, Enhancement of CO2 conversion in microwave plasmas using a nozzle in the effluent, Journal of CO2 Utilization 57 (2022) 101870. https://doi.org/10.1016/j.jcou.2021.101870.
[6] S. Van Alphen, A. Hecimovic, C.K. Kiefer, U. Fantz, R. Snyders, A. Bogaerts, Modelling post-plasma quenching nozzles for improving the performance of CO2 microwave plasmas, Chemical Engineering Journal 462 (2023) 142217. https://doi.org/https://doi.org/10.1016/j.cej.2023.142217.
[7] V. Vermeiren, A. Bogaerts, Plasma-Based CO2 Conversion: To Quench or Not to Quench?, The Journal of Physical Chemistry C 124(34) (2020) 18401-18415. https://doi.org/10.1021/acs.jpcc.0c04257.
[8] T.L.E.C. Systems, Concepts of signal noise reduction - Shielding and grounding, 2013. https://torchmate.com/news/Concepts-of-Signal-Noise-Reduction. (Accessed 31 January 2023).
[9] P. Mazurek, Chosen Aspects of the Electromagnetic Compatibility of Plasma Reactors with Gliding Arc Discharges, Applied Sciences 10(11) (2020) 3789. https://doi.org/10.3390/app10113789.